

Distinct topological crystalline phases in models for the strongly correlated topological insulator SmB_6

Pier Paolo Baruselli and Matthias Vojta

Institut für Theoretische Physik, Technische Universität Dresden, 01062 Dresden, Germany

(Dated: May 13, 2015)

SmB_6 was recently proposed to be both a strong topological insulator and a topological crystalline insulator. For this and related cubic topological Kondo insulators, we prove the existence of four different topological phases, distinguished by the sign of mirror Chern numbers. We characterize these phases in terms of simple observables, and we provide concrete tight-binding models for each phase. Based on theoretical and experimental results for SmB_6 we conclude that it realizes the phase with $C_{k_z=0}^+ = +2$, $C_{k_z=\pi}^+ = +1$, $C_{k_x=k_y}^+ = -1$, and we propose a corresponding minimal model.

Topological insulators (TIs) with strong electronic correlations are considered to be of crucial importance in the exciting field of topological phases: They may provide TI states which are truly bulk-insulating – a property missing from many Bi-based TIs – and they may host novel and yet unexplored interaction-driven phenomena.

In this context, the material SmB_6 has attracted enormous attention: it has been proposed [1–3] to realize a three-dimensional (3D) topological Kondo insulator (TKI). This is a system where f -electron local moments form at intermediate temperatures T and are subsequently screened at low T , such that a topologically non-trivial bandstructure emerges from Kondo screening [4].

While the results of numerous experiments on SmB_6 , such as transport [5–7] and quantum oscillation measurements [8] as well as angle-resolved photoemission spectroscopy (ARPES) [9–13] and spin-resolved ARPES (SP-ARPES) [14], appear consistent with the presence of Dirac-like surface states expected in a TKI, doubts have been raised about the proper interpretation of data [15–17]. Clearly, both experimental and theoretical progress is required for a thorough comprehension of this material.

A recent theoretical insight [18] is that SmB_6 is also a topological crystalline insulator (TCI) [19], having three non-zero mirror Chern numbers. While Ref. 18 concluded that the latter are, modulo 2 or 4, independent of model details, we show in this Letter that the individual values of these Chern numbers do depend on model details. As a result, we obtain four distinct TCI phases which in particular differ in their surface-state spin structure. Using results from density-functional theory (DFT) and SP-ARPES we are able to single out one of the four phases as being relevant for SmB_6 . We also show that some of the previously employed models [3, 20] do not belong to this phase, and we propose a new minimal model for the correct TCI phase. Our results highlight the non-trivial role played by mirror Chern numbers in describing topological band structures of actual materials.

Lattice and symmetries. SmB_6 crystallizes in a simple-cubic (*sc*) structure, with its first Brillouin zone (BZ) shown in Fig. 1(a). In the following we use the lattice spacing $a = 4.13 \text{ \AA}$ as unit length. We may introduce mir-

ror operators $M_l \equiv PC_2(l)$, where P is the inversion and $C_2(l)$ is a rotation by π about the axis l perpendicular to the mirror plane. For spin-1/2 particles $M_l^2 = -1$, such that M_l operators have eigenvalues $\pm i$. For cubic symmetry there are three independent momentum-space planes which are invariant under the relevant mirror operators: the planes $k_z = 0$ (equivalent to $k_{x,y} = 0$) and $k_z = \pi$ (equivalent to $k_{x,y} = \pi$) are invariant under M_z while the plane $k_x = k_y$ (equivalent to $k_x = -k_y$, $k_y = \pm k_z$, $k_z = \pm k_x$) is invariant under M_{x-y} ; see Fig. 1(a).

Topological invariants. For each momentum-space mirror plane, one can define a mirror Chern number [18]:

$$C_{B\bar{Z}}^\pm = \frac{i}{2\pi} \sum_{a,b=1}^2 \epsilon_{ab} \sum_{n=1}^N \int_{B\bar{Z}} d^2\mathbf{k} \langle \partial_a u_n^\pm(\mathbf{k}) | \partial_b u_n^\pm(\mathbf{k}) \rangle, \quad (1)$$

with $M|u_n^\pm(\mathbf{k})\rangle = \pm i|u_n^\pm(\mathbf{k})\rangle$ and \mathbf{k} lying in the plane $B\bar{Z}$ which is invariant under the symmetry operator M ($M=M_z$ when $B\bar{Z}$ is $k_z = 0$ or $k_z = \pi$, $M=M_{x-y}$ when $B\bar{Z}$ is $k_x = k_y$), and we sum over all N occupied bands. We note that $C_{B\bar{Z}}^+ + C_{B\bar{Z}}^- = 0$ and, by cubic symmetry,

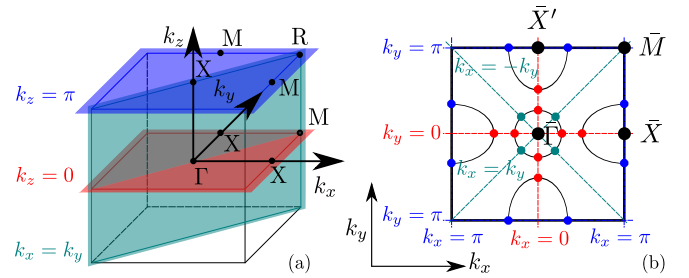


Figure 1. (a) 3D BZ and its mirror planes $k_z = 0$, $k_z = \pi$, $k_x = k_y$; high-symmetry points are $\Gamma = (0, 0, 0)$, $X = (\pi, 0, 0)$, $(0, \pi, 0)$, $M = (0, \pi, \pi)$, $(\pi, 0, \pi)$, $R = (\pi, \pi, \pi)$. (b) Corresponding 2D BZ for a (001) surface with its high-symmetry points $\bar{\Gamma} = (0, 0)$, $\bar{X} = (\pi, 0)$, $\bar{X}' = (0, \pi)$ and $\bar{M} = (\pi, \pi)$ and its mirror planes $k_{x,y} = 0$, $k_{x,y} = \pi$, $k_x = \pm k_y$, which are pairwise equivalent by C_{4v} symmetry. (Planes at $k_{x,y} = \pi$ and $k_{x,y} = -\pi$ are identical and share a single label.) Also shown is the 2D Fermi surface of SmB_6 , consisting of three pockets centered at $\bar{\Gamma}$, \bar{X} , and \bar{X}' . Dots mark its intersections with mirror planes.

Model	Abbr.	N_{bands}	Basis	Parameters				$C_{k_z=0}^+$	$C_{k_z=\pi}^+$	$C_{k_x=k_y}^+$	v	w	Fig. 2
Γ_8 1NN hyb.	Γ_8^{1x}	8	E_g, Γ_8	$\epsilon^f - \epsilon^d$	η_z^{d1}, η_z^{d2}	η_z^{f1}, η_z^{f2}	η_x^{v1}	-2	+1	+1	-1	-1	(a)
Γ_7 2NN hyb.	Γ_7^{2z}	6	E_g, Γ_7	$\epsilon^f - \epsilon^d$	η_z^{d1}, η_z^{d2}	η_7^{f2}, η_7^{f3}	η_7^{v2}	-2	+1	+1	-1	-1	(a)*
Γ_8 2NN hyb.	Γ_8^{2z}	8	E_g, Γ_8	$\epsilon^f - \epsilon^d$	η_z^{d1}, η_z^{d2}	η_z^{f1}, η_z^{f2}	η_z^{v2}	+2	+1	-1	-1	+1	(b)
Γ_7 1NN hyb.	Γ_7^{1x}	6	E_g, Γ_7	$\epsilon^f - \epsilon^d$	η_z^{d1}, η_z^{d2}	η_7^{f2}, η_7^{f3}	η_7^{v1}	+2	+1	-1	-1	+1	(b)*
Full tight-binding [21, 22]	FTB	10	E_g, Γ_8, Γ_7	many				+2	+1	-1	-1	+1	(b)
Alexandrov [3] 1NN hyb.	A^{1z}	8	E_g, Γ_8	$\epsilon^f - \epsilon^d$	η_z^{d1}, η_x^{d1}	η_z^{f1}, η_x^{f1}	η_z^{v1}	-2	+1	-1	+1	-1	(c)
Legner et al. [20]	sf	4	$s, \Gamma_8^{(2)}$	$\epsilon^f - \epsilon^s$	η^{s1}, η^{s2}	η^{f1}, η^{f2}	η^{v1}	-2	+1	-1	+1	-1	(c)
Alexandrov [3] 2NN hyb.	A^{2x}	8	E_g, Γ_8	$\epsilon^f - \epsilon^d$	η_z^{d1}, η_x^{d1}	η_z^{f1}, η_x^{f1}	η_x^{v2}	+2	+1	+1	+1	+1	(d)

Table I. Mirror Chern numbers $C_{k_z=0}^+$, $C_{k_z=\pi}^+$, $C_{k_x=k_y}^+$ in different tight-binding models for SmB₆, with 1NN (2NN) referring to first (second) neighbor hybridization. Also quoted are the number of bands N_{bands} , the orbital basis, and the non-zero terms in the Hamiltonian required by each model (divided into on-site energies ϵ , d hopping η^d , f hopping η^f , hybridization η^v) [23]. The four phases, distinguished by $v \equiv \text{sgn}(C_{k_z=0}^+ C_{k_x=k_y}^+)$ and $w \equiv \text{sgn}(C_{k_z=0}^+ C_{k_z=\pi}^+)$, are illustrated in Fig. 2 (where for Γ_7 models* the spin directions needs to be reversed).

$C_{k_z=0}^+ = C_{k_x=0}^+ = C_{k_y=0}^+$ etc. A given insulating band-structure is thus characterized by a triplet of numbers $(C_{k_z=0}^+, C_{k_z=\pi}^+, C_{k_x=k_y}^+)$.

We recall that, according to bandstructure calculations [1, 2], SmB₆ is a strong TI: Band inversion between d and f states is achieved at the three X points of the 3D BZ, leading to the parity invariants [24] $\delta(\Gamma) = +1$, $\delta(X) = -1$, $\delta(M) = +1$, $\delta(R) = +1$ and to the \mathbb{Z}_2 indices $(\nu_0, \nu_1 \nu_2 \nu_3) = (1, 111)$. Ref. 18 proved, using the properties of the wavefunctions at high-symmetry points, that the mirror Chern numbers of SmB₆ obey $C_{k_z=0}^+ = 2 \bmod 4$, $C_{k_z=\pi}^+ = 1 \bmod 4$, $C_{k_x=k_y}^+ = 1 \bmod 2$ *independent* of microscopic details (like the \mathbb{Z}_2 indices). Below we show this does *not* apply to the individual values of these Chern numbers which instead are model-dependent.

Tight-binding models. Ab-initio bandstructure calculations for SmB₆ [2, 21, 25] show that the bands close to the Fermi energy originate from Sm orbitals, namely in the d shell the E_g quartet $|d_{x^2-y^2} \uparrow\rangle$, $|d_{x^2-y^2} \downarrow\rangle$, $|d_{z^2} \uparrow\rangle$, $|d_{z^2} \downarrow\rangle$ and in the f shell, where strong spin-orbit coupling pushes the $j = 7/2$ multiplet well above the Fermi energy, the $j = 5/2$ multiplet, which is split by cubic crystal field into a Γ_8 quartet, $|\Gamma_8^{(1)} \pm\rangle = \sqrt{\frac{5}{6}}|\pm \frac{5}{2}\rangle + \sqrt{\frac{1}{6}}|\mp \frac{3}{2}\rangle$, $|\Gamma_8^{(2)} \pm\rangle = |\pm \frac{1}{2}\rangle$, and a Γ_7 doublet, $|\Gamma_7 \pm\rangle = \sqrt{\frac{1}{6}}|\pm \frac{5}{2}\rangle - \sqrt{\frac{5}{6}}|\mp \frac{3}{2}\rangle$. Any reasonable model must thus consist of a sc lattice of Sm atoms, but the choice of included orbitals and tight-binding parameters (on-site energies ϵ and hopping parameters η) is not univocal. In fact, published papers employed models with either 10 bands (E_g, Γ_8, Γ_7) [22], or 8 bands (E_g, Γ_8) [3, 22], or 6 bands (E_g, Γ_7) [22], or 4 bands (s doublet, $\Gamma_8^{(2)}$ doublet) [20]. Once the basis orbitals are fixed, different sets of hopping parameters η may be used: in Table I we summarize some of these choices, with details given in the supplement [26].

We note that our discussion will be exclusively based

on single-particle models: Although the Hubbard repulsion among f electrons is not small, its effect at low temperatures can be captured in terms of renormalized f -electron kinetic energy and hybridization [27]. Hence, we can think of working directly with renormalized parameters; our qualitative conclusions are independent of interaction-induced renormalizations.

Distinct topological phases. Our main finding is that, upon computing mirror Chern numbers for different SmB₆ models, $C_{k_z=0}^+$ can be either +2 or -2 and $C_{k_x=k_y}^+ = +1$ or -1, while $C_{k_z=\pi}^+ = +1$ always. This yields a total of four distinct phases, summarized in Table I. In particular, models from Ref. 3 (here denoted as A^{1z}) and Ref. 20 (sf) are found to belong to the $(-2, +1, -1)$ phase, while models from Ref. 22 with Γ_7 and/or Γ_8 multiplets realize either the $(+2, +1, -1)$ or the $(-2, +1, +1)$ phase; the $(+2, +1, +1)$ phase is finally achieved in model A^{2x} obtained by modifying the hybridization term in model A^{1z} from Ref. 3.

Phases and symmetries of surface states. In order to give a transparent physical meaning to the four phases, we relate the mirror Chern numbers to the properties of topological surface states. First, the absolute value of a mirror Chern number reflects the (minimum) number of Dirac points arising along a high-symmetry line in the 2D surface BZ [18, 20, 24]. For instance, on the (001) surface there are two Dirac points along the $k_{x,y} = 0$ directions, and one along $k_{x,y} = \pi$ and $k_x = \pm k_y$; see Fig. 1(b). This is consistent with the three Dirac cones at $\bar{\Gamma}$, \bar{X} and \bar{X}' predicted by parity invariants [1–3] and observed experimentally [9–13]. Apparently, the absolute values of the C yield no additional information for the (001) surface (but they do for the (011) one [18]). This also shows that no other TCI phases are possible, since they would give rise to more Dirac cones than actually observed.

However, the sign of a mirror Chern number gives new information, as it fixes the mirror-symmetry eigenvalue of surface states. For example, $C_{k_z=0}^+ = C_{k_x=0}^+ = +2$

tells that along $k_x = 0$ there are two bands with positive velocity along the $\hat{z} \times \hat{x} = \hat{y}$ direction and M_x eigenvalues $+i$, while for $C_{k_z=0}^+ = -2$ these states have eigenvalue $-i$ [20, 24]. By a repeated use of this property we can assign all the $\pm i$ eigenvalues in Fig. 2(a)–(d) for the four possible phases.

Surface-state spin structure. Since mirror eigenvalues are not directly measurable, we now link them to the spin expectation value (SEV) of surface states as observable in SP-ARPES experiments [14]. The idea is as follows: If each Dirac-cone state would simply behave as a spin-1/2 state with $M_l = C_2(l) = e^{-i\pi\sigma_l} = -i\sigma_l$, we would have $M_l|s_l\rangle = -i\sigma_l|s_l\rangle = -i s_l|s_l\rangle$ ($l = x, y, x \pm y$), with $|s_l\rangle$ an eigenvector of the Pauli matrix σ_l with eigenvalue $s_l = \pm 1$. Hence, M_l eigenvalues of $\pm i$ would immediately give the direction of the spin, e.g., an M_x eigenvalue of $-i$ would imply a spin pointing towards $+x$. However, additional minus signs arise for orbitals odd under M_l , and, due to the spin-orbit coupling in the f shell, surface states are not eigenstates of spin operators. By explicitly invoking the properties of the basis states we can derive rules relating the mirror eigenvalues to the SEV: We find that $M_l|\psi\rangle = -i|\psi\rangle$ implies that the SEV for state $|\psi\rangle$ points along direction $\pm l$, with the plus sign always holding except for $M_{x\pm y}$ acting on $d_{x^2-y^2}$ and $\Gamma_8^{(1)}$ states and for $M_{x,y}$ on Γ_7 states [26]. Using these rules, and the fact that for small momenta around $\bar{\Gamma}$ the SEV does not depend on the eigenvalues of $M_{x\pm y}$ (see below), we can construct a full portrait of the SEV for each phase once a basis has been fixed, see Fig. 2 for Γ_8 states.

We proceed by analyzing these portraits in detail. Interpreting the SEV in Fig. 2 as true spin [28], the effective low-energy model at the \bar{X} points can be written as:

$$H_{\bar{X}} = v_1(k_x - \pi)\sigma_y - v_2k_y\sigma_x, \quad (2)$$

$$H_{\bar{X}'} = v_2k_x\sigma_y - v_1(k_y - \pi)\sigma_x. \quad (3)$$

Importantly, the velocities $v_{1,2}$ have the same (opposite) sign if $C_{k_z=0}^+C_{k_z=\pi}^+ > 0$ (< 0), respectively. We introduce $w \equiv \text{sgn}(C_{k_z=0}^+C_{k_z=\pi}^+) = \text{sgn}(v_1v_2)$ which describes how the mirror eigenvalues and the SEV on the \bar{X} cones evolve upon $\pi/2$ momentum-space rotations around \bar{X} . This implies that w is a *winding number*: when $w = +1$ spin and momentum rotate around \bar{X} in the same direction, Figs. 2(b,d), while for $w = -1$ they rotate in the opposite direction, Figs. 2(a,c). We note that $w = -1$ is only allowed for cones at low-symmetry points, see below.

Similarly, we introduce $v \equiv \text{sgn}(C_{k_z=0}^+C_{k_x=k_y}^+)$ which now describes how the mirror eigenvalues on the $\bar{\Gamma}$ cone evolve upon $\pi/4$ rotations. It turns out, however, that v does not affect the SEV of the $\bar{\Gamma}$ cone: For sufficiently small momenta the system must display continuous rotation symmetry around $\bar{\Gamma}$ which implies a fixed angle between SEV and momentum along the contour (i.e., a winding number $+1$). Thus the effective low-energy

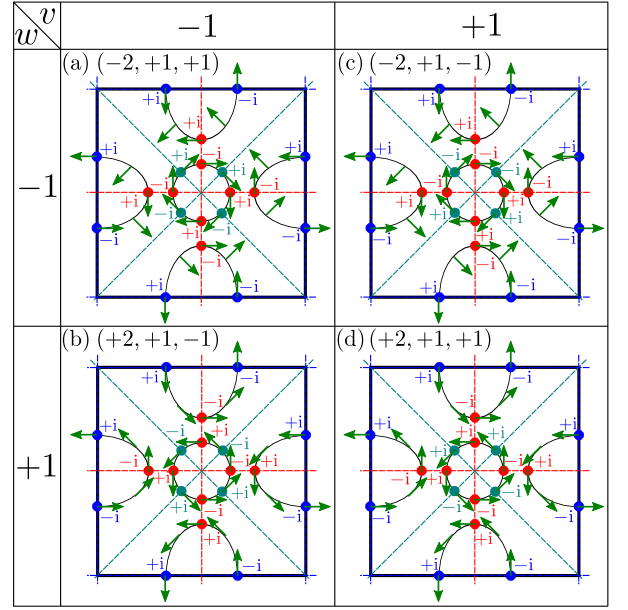


Figure 2. Surface-state mirror eigenvalues $\pm i$ (defined at surface momenta where the Fermi contour crosses a mirror plane) for the four phases with mirror Chern numbers ($C_{k_z=0}^+, C_{k_z=\pi}^+, C_{k_x=k_y}^+$) as quoted in the panels. The C signs can be condensed into $v \equiv \text{sgn}(C_{k_z=0}^+C_{k_x=k_y}^+)$ and $w \equiv \text{sgn}(C_{k_z=0}^+C_{k_z=\pi}^+)$, see text. Green arrows show the surface-state SEV for Γ_8 states; for Γ_7 states (see Table I for models) it would be reversed. In the FTB model this reversal depends on the relative weight of Γ_7 and Γ_8 states, with Γ_8 dominating for realistic parameters [22].

model at the $\bar{\Gamma}$ point is independent of v , and reads

$$H_{\bar{\Gamma}} = v_0w(k_x\sigma_y - k_y\sigma_x) \quad (v_0 > 0), \quad (4)$$

with spin and momentum always forming a mutual angle $\pm\pi/2$ given by the sign of v_0w , i.e., the chirality. We note that the w factor in $H_{\bar{\Gamma}}$ is needed to give the correct relative spin direction along k_x and k_y between the $\bar{\Gamma}$ and the \bar{X} cones, which is fixed by $|C_{k_z=0}^+| = 2$. Using $H_{\bar{\Gamma}}$ we can show [26] that v instead dictates symmetry properties of the states composing the $\bar{\Gamma}$ cone for small momenta: for $v = +1$ these are d_{z^2} and $\Gamma_8^{(2)}$ (X_6 symmetry representation) whereas for $v = -1$ these are $d_{x^2-y^2}$, $\Gamma_8^{(1)}$ and Γ_7 (corresponding to X_7).

Relation between v, w and electronic structure. In order to determine the TCI phase of SmB_6 we now connect the parameters v and w to the bulk bandstructure. Surface states near $\bar{\Gamma}$ can be computed by perturbatively expanding the Hamiltonian around $X = (0, 0, \pi)$ [29, 30], where it decouples into a subspace with symmetry representation X_7 , composed from $d_{x^2-y^2}$, $\Gamma_8^{(1)}$, and Γ_7 states, and a subspace with symmetry representation X_6 and d_{z^2} , $\Gamma_8^{(2)}$ states. Band inversion can be achieved in only one of these subspaces: in model A^{1z} from Refs. 3 and 30 it is assumed to be in the subspace X_6 , while DFT calcu-

lations [25] display band inversion in subspace X_7 . Since surface states at $\bar{\Gamma}$ only exist in the subspace where band inversion is achieved [30], and this depends on which d band has a minimum at X , we can link these two options to the symmetry of the d -band minimum at X : d_{z^2} (X_6^+) in the first case, leading to $v = +1$, $d_{x^2-y^2}$ (X_7^+) in the second, leading to $v = -1$. Since we expect DFT to be reliable for weakly correlated orbitals, we conclude that $v = -1$ in real SmB_6 .

Once the band-inversion subspace, and thus v , is fixed by the choice of the hopping terms, w depends on the hybridization term: out of those which lead to a full gap, some lead to $w = +1$, some others to $w = -1$, as shown in Table I. When considering Γ_8 states, DFT calculations [21, 22] show the largest of the hybridization terms to be η_z^{v1} [23], which, however, alone does not lead to a gap for $v = -1$, since it does not couple the inverted bands $d_{x^2-y^2}$ and $\Gamma_8^{(1)}$ along Γ - X for symmetry reasons. The second-largest term is η_z^{v2} , which gives $w = +1$ (Γ_8^{2z} in Table I). However, a competition with the $w = -1$ phase can be observed when retaining both Γ_7 and Γ_8 multiplets [22], since the Γ_7 doublet alone with E_g is in the $w = -1$ phase, η_7^{v2} being the largest hybridization term in this case (Γ_7^{2z}).

Choice of phase and minimal model. We now make use of the following ingredients: (i) The band inversion properties from DFT calculations yield $v = -1$. (ii) The SP-ARPES experiment of Ref. 14 shows a winding number on \bar{X} cones of $w = +1$. Together, this uniquely yields $(+2, +1, -1)$ as the best candidate TCI phase for SmB_6 .

At the same time, we realize that the Γ_8^{2z} model, obtained retaining the E_g and Γ_8 quartets, with $\eta_z^{d2}/\eta_z^{d1} \sim \eta_z^{f2}/\eta_z^{f1} \sim -3/8$ and the η_z^{v2} hybridization term, is the simplest one giving the correct mirror Chern numbers $(+2, +1, -1)$ and reproducing as closely as possible the DFT bandstructure. We propose it as a new minimal model for SmB_6 , with a concrete tight-binding parametrization given in the supplement [26]. We stress that this conclusion is based on the experimental result $w = +1$; $w = -1$ would instead lead to a minimal model entailing the E_g quartet and the Γ_7 doublet (Γ_7^{2z}). The competition between the $w = +1$ and $w = -1$ phases, emerging from the Γ_8 quartet and the Γ_7 doublet, respectively, depends on model details which have not been obtained with sufficient accuracy from DFT. This applies for instance to the Γ_7 - Γ_8 energy difference whose variation can drive a topological phase transition between states with different w .

Quasiparticle interference (QPI). QPI can be used as a probe of the topological character of surface states [31–33], owing to their spin texture; in TCIs, impurities which do not break mirror symmetries cannot induce transitions between states with opposite mirror eigenvalues [34]. Here we show how the winding number w affects intercone scattering. Comparing the spin portraits for two relevant models in Figs. 3(a) and (c) we see that, for

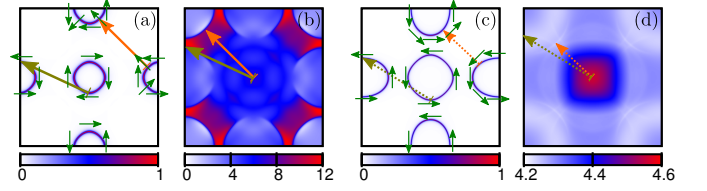


Figure 3. Isoenergy contours with SEV (a,c) and QPI signal (b,d) at the Fermi level for two different SmB_6 tight-binding models. Large arrows show intercone scattering wavevectors. (a,b): Four-band model sf in the $(-2, +1, -1)$ phase ($w = -1$); (c,d): Eight-band model Γ_8^{2z} in the $(+2, +1, -1)$ phase ($w = +1$); with parameters given in the supplement [26]. An intercone QPI signal is seen in (b), but not in (d), dictated by the surface-state spin structure.

pairs of stationary points [35] (states which have the same tangent to the isoenergy contour) belonging to different \bar{X} cones, $w = -1$ ($w = +1$) implies roughly parallel (antiparallel) spin, respectively. Consequently, $w = -1$ yields a QPI peak from intercone scattering [36, 37], Fig. 3(b), while $w = +1$ does not [22], Fig. 3(d). Thus, QPI can probe w by looking at intercone scattering, and hence provides information on the spin structure of the Dirac cones and, indirectly, on mirror Chern numbers.

Conclusions. In this Letter we have studied mirror Chern numbers in different models for the correlated topological insulator SmB_6 . The absolute values of the mirror Chern numbers are fixed by symmetry properties of the atomic orbitals and the bandstructure and are thus independent of model details, while their signs are model-dependent. This yields four possible phases – all sharing the \mathbb{Z}_2 topological indices $(1,111)$ – which can be characterized by the two combinations of signs $v \equiv \text{sgn}(\mathcal{C}_{k_z=0}^+ \mathcal{C}_{k_x=k_y}^+)$ and $w \equiv \text{sgn}(\mathcal{C}_{k_z=0}^+ \mathcal{C}_{k_z=\pi}^+)$. These have a straightforward physical interpretation in terms of the symmetry of the d -band minimum at X and the spin texture of the \bar{X} cone on a (001) surface, respectively. Our analysis constrains SmB_6 to be in the $(\mathcal{C}_{k_z=0}^+, \mathcal{C}_{k_z=\pi}^+, \mathcal{C}_{k_x=k_y}^+) = (+2, +1, -1)$ phase, by using the results of DFT calculations and of SP-ARPES [14] which give $v = -1$ and $w = +1$, respectively. For the $w = +1$ case we predict a weak QPI signal from intercone scattering.

From our analysis we propose a minimal tight-binding model for SmB_6 consisting of 8 orbitals (the E_g and Γ_8 quartets). The model equals the one of Ref. 3 in the choice of the orbital basis but differs in both the kinetic energy and the hybridization parameters; it better reproduces DFT and SP-ARPES data, at the price of introducing second-neighbor hopping parameters. We finally speculate that chemical substitution can tune both the Γ_7 - Γ_8 energy difference and the hopping parameters, possibly leading to a topological phase transition from the $w = +1$ to the $w = -1$ state. Such a transition is accompanied by the closing of the bulk gap.

We believe that our results advance the understanding of the complex TKI material SmB_6 (and its cousin PuB_6 [21]), and potentially of other TIs, too.

This research was supported by the DFG through SFB 1143 and GRK 1621 as well as by the Helmholtz association through VI-521.

Note added: At the day of submission of this paper, a related paper [38] appeared on arXiv, which reaches conclusions compatible with ours. For comparison we note that their Chern number C_d equals our $(-C_{k_x=k_y}^+)$.

-
- [1] T. Takimoto, J. Phys. Soc. Jpn. **80**, 123710 (2011).
[2] F. Lu, J. Zhao, H. Weng, Z. Fang, and X. Dai, Phys. Rev. Lett. **110**, 096401 (2013).
[3] V. Alexandrov, M. Dzero, and P. Coleman, Phys. Rev. Lett. **111**, 226403 (2013).
[4] M. Dzero, K. Sun, V. Galitski, and P. Coleman, Phys. Rev. Lett. **104**, 106408 (2010).
[5] S. Wolgast, C. Kurdak, K. Sun, J. W. Allen, D.-J. Kim, and Z. Fisk, Phys. Rev. B **88**, 180405(R) (2013).
[6] D. J. Kim, J. Xia, and Z. Fisk, Nature Mat. **13**, 466 (2014).
[7] X. Zhang, N. P. Butch, P. Syers, S. Ziemak, R. L. Greene, and J. Paglione, Phys. Rev. X **3**, 011011 (2013).
[8] G. Li, Z. Xiang, F. Yu, T. Asaba, B. Lawson, P. Cai, C. Tinsman, A. Berkley, S. Wolgast, Y. S. Eo, D.-J. Kim, C. Kurdak, J. W. Allen, K. Sun, X. H. Chen, Y. Y. Wang, Z. Fisk, and L. Li, Science **346**, 1208 (2014).
[9] M. Neupane, N. Alidoust, S. Xu, T. Kondo, Y. Ishida, D.-J. Kim, C. Liu, I. Belopolski, Y. Jo, T.-R. Chang, H.-T. Jeng, T. Durakiewicz, L. Balicas, H. Lin, A. Bansil, S. Shin, Z. Fisk, and M. Z. Hasan, Nature Comm. **4**, 2991 (2013).
[10] N. Xu, X. Shi, P. K. Biswas, C. E. Matt, R. S. Dhaka, Y. Huang, N. C. Plumb, M. Radovic, J. H. Dil, E. Pomjakushina, K. Conder, A. Amato, Z. Salman, D. M. Paul, J. Mesot, H. Ding, and M. Shi, Phys. Rev. B **88**, 121102 (2013).
[11] J. Jiang, S. Li, T. Zhang, Z. Sun, F. Chen, Z. Ye, M. Xu, Q. Ge, S. Tan, X. Niu, M. Xia, B. Xie, Y. Li, X. Chen, H. Wen, and D. Feng, Nature Comm. **4**, 2991 (2013).
[12] C.-H. Min, P. Lutz, S. Fiedler, B. Kang, B. Cho, H.-D. Kim, H. Bentmann, and F. Reinert, Phys. Rev. Lett. **112**, 226402 (2014).
[13] J. D. Denlinger, J. W. Allen, J.-S. Kang, K. Sun, B.-I. Min, D.-J. Kim, and Z. Fisk, preprint arXiv:1312.6636.
[14] N. Xu, P. K. Biswas, J. H. Dil, R. S. Dhaka, G. Landolt, S. Muff, C. E. Matt, X. Shi, N. C. Plumb, M. Radovic, E. Pomjakushina, K. Conder, A. Amato, S. Borisenko, R. Yu, H.-M. Weng, Z. Fang, X. Dai, J. Mesot, H. Ding, and M. Shi, Nature Comm. **5**, 4566 (2014).
[15] Z.-H. Zhu, A. Nicolaou, G. Levy, N. P. Butch, P. Syers, X. F. Wang, J. Paglione, G. A. Sawatzky, I. S. Elfimov, and A. Damascelli, Phys. Rev. Lett. **111**, 216402 (2013).
[16] E. Frantzeskakis, N. de Jong, B. Zwartsenberg, Y. K. Huang, Y. Pan, X. Zhang, J. X. Zhang, F. X. Zhang, L. H. Bao, O. Tegus, A. Varykhalov, A. de Visser, and M. S. Golden, Phys. Rev. X **3**, 041024 (2013).
[17] P. Hlawenka, K. Siemensmeyer, E. Weschke, A. Varykhalova, J. Sanchez-Barriga, N. Y. Shitsevalova, A. V. Dukhnenko, V. B. Filipov, S. Gabni, K. Flachbart, O. Rader, and E. D. L. Rienks, preprint arXiv:1502.01542.
[18] M. Ye, J. W. Allen, and K. Sun, preprint arXiv:1307.7191.
[19] L. Fu, Phys. Rev. Lett. **106**, 106802 (2011).
[20] M. Legner, A. Rüegg, and M. Sigrist, Phys. Rev. B **89**, 085110 (2014).
[21] X. Deng, K. Haule, and G. Kotliar, Phys. Rev. Lett. **111**, 176404 (2013).
[22] P. P. Baruselli and M. Vojta, Phys. Rev. B **90**, 201106 (2014).
[23] We denote the η parameters as follows: the superscript denotes the d , s or f shell for the kinetic energy, and v for the hybridization, and the layer of NN; the subscript, if it involves $d_{x^2-y^2}$ or $\Gamma_8^{(1)}$ along the 001 or 110 direction, is x , if it involves d_{z^2} or $\Gamma_8^{(2)}$ along the 100 or 011 direction, is z , if it involves Γ_7 is 7. So, for example, η_z^{v1} is the 1NN hybridization term along 001 between d_{z^2} and $\Gamma_8^{(2)}$.
[24] J. C. Y. Teo, L. Fu, and C. L. Kane, Phys. Rev. B **78**, 045426 (2008).
[25] C.-J. Kang, J. Kim, K. Kim, J. Kang, J. D. Denlinger, and B. I. Min, Journal of the Physical Society of Japan **84**, 024722 (2015).
[26] In the Supplemental material we give details about the model definition, the SEV from mirror-symmetry eigenvalues, and the symmetry of surface states at $\bar{\Gamma}$.
[27] A. C. Hewson, *The Kondo Problem to Heavy Fermions* (Cambridge University Press, Cambridge, 1993).
[28] In a microscopic quantitative treatment[29], Pauli matrices will rather describe a Kramer's pair $|\psi_+\rangle$, $|\psi_-\rangle$ whose SEV is such that $|\psi_+\rangle \sim |\uparrow\rangle$, $|\psi_-\rangle \sim |\downarrow\rangle$, but our qualitative conclusions will not change.
[29] C.-X. Liu, X.-L. Qi, H. Zhang, X. Dai, Z. Fang, and S.-C. Zhang, Phys. Rev. B **82**, 045122 (2010).
[30] B. Roy, J. D. Sau, M. Dzero, and V. Galitski, Phys. Rev. B **90**, 155314 (2014).
[31] T. Zhang, P. Cheng, X. Chen, J.-F. Jia, X. Ma, K. He, L. Wang, H. Zhang, X. Dai, Z. Fang, X. Xie, and Q.-K. Xue, Phys. Rev. Lett. **103**, 266803 (2009).
[32] P. Roushan, J. Seo, C. V. Parker, Y. S. Hor, D. Hsieh, D. Qian, A. Richardella, and M. Z. Hasan, Nature **460**, 1106 (2009).
[33] H.-M. Guo and M. Franz, Phys. Rev. B **81**, 041102 (2010).
[34] C. Fang, M. J. Gilbert, S.-Y. Xu, B. A. Bernevig, and M. Z. Hasan, Phys. Rev. B **88**, 125141 (2013).
[35] Q. Liu, X.-L. Qi, and S.-C. Zhang, Phys. Rev. B **85**, 125314 (2012).
[36] P. P. Baruselli and M. Vojta, Phys. Rev. B **89**, 205105 (2014).
[37] R. Yu, H. Weng, X. Hu, Z. Fang, and X. Dai, New J. Phys. **17**, 023012 (2015).
[38] M. Legner, A. Rüegg, and M. Sigrist, preprint arXiv:1505.02987.

Supplemental material for “Distinct topological crystalline phases in models for the strongly correlated topological insulator SmB₆”

Pier Paolo Baruselli and Matthias Vojta

Institut für Theoretische Physik, Technische Universität Dresden, 01062 Dresden, Germany

I. MODEL HAMILTONIANS

In this section we provide explicit expressions for the tight-binding Hamiltonians referred to in the main text and Table 1.

A. Parametrization

We will use σ , τ , and μ Pauli matrices as follows: σ matrices act in the (pseudo)spin subspace, τ in the orbital subspace, and μ in the d - f subspace. Then, terms proportional to μ_0 and μ_z denote the kinetic energy (with

subscript 0 representing the 2×2 unit matrix) while terms proportional to μ_y correspond to d - f hybridization. For convenience, we introduce $\mu_1 = (\mu_0 + \mu_z)/2$, $\mu_2 = (\mu_0 - \mu_z)/2$, $\tau_1 = (\tau_0 + \tau_z)/2$, $\tau_2 = (\tau_0 - \tau_z)/2$: μ_1 projects onto the d subspace, μ_2 onto the f subspace, τ_1 onto the orbital subspace 1 ($d_{x^2-y^2}$, $\Gamma_8^{(1)}$), and τ_2 onto the orbital subspace 2 (d_{z^2} , $\Gamma_8^{(2)}$). We also employ abbreviations $c_x = \cos k_x$, $c_y = \cos k_y$, $c_z = \cos k_z$, $s_x = \sin k_x$, $s_y = \sin k_y$, $s_z = \sin k_z$.

We consider three classes of models:

- 8-band models consisting of the $E_g(d)$ quartet interacting with the $\Gamma_8(f)$ quartet.

The parameters are $\epsilon^d = \langle d_{x^2-y^2} | H | d_{x^2-y^2} \rangle_{000} = \langle d_{z^2} | H | d_{z^2} \rangle_{000}$, $\epsilon_8^f = \langle \Gamma_8^{(1)} + |H| \Gamma_8^{(1)} \rangle_{000} = \langle \Gamma_8^{(2)} + |H| \Gamma_8^{(2)} \rangle_{000}$, $\eta_x^{d1} = \langle d_{x^2-y^2} | H | d_{x^2-y^2} \rangle_{001}$, $\eta_z^{d1} = \langle d_{z^2} | H | d_{z^2} \rangle_{001}$, $\eta_z^{d2} = \langle d_{z^2} | H | d_{z^2} \rangle_{110}$, $\eta_x^{f1} = \langle \Gamma_8^{(1)} + |H| \Gamma_8^{(1)} \rangle_{001}$, $\eta_z^{f1} = \langle \Gamma_8^{(2)} + |H| \Gamma_8^{(2)} \rangle_{001}$, $\eta_z^{f2} = \langle \Gamma_8^{(2)} + |H| \Gamma_8^{(2)} \rangle_{110}$, $\eta_x^{v1} = \langle d_{x^2-y^2} \uparrow | H | \Gamma_8^{(1)} \rangle_{001}$, $\eta_z^{v1} = \langle d_{z^2} \uparrow | H | \Gamma_8^{(2)} \rangle_{001}$, $\eta_x^{v2} = \langle d_{x^2-y^2} \uparrow | H | \Gamma_8^{(1)} \rangle_{110}$, $\eta_z^{v2} = \langle d_{z^2} \uparrow | H | \Gamma_8^{(2)} \rangle_{110}$, and Hamiltonian $H = H_{E_g} + H_{\Gamma_8} + V_{E_g-\Gamma_8}$:

$$H_i(\mathbf{k}) = \epsilon^i \tau_0 \sigma_0 \mu_i - t_i \sigma_0 \mu_i \cdot \{ [(c_x + c_y + c_z)(\eta_z^{i1} + \eta_x^{i1}) + 2\eta_z^{i2}(c_x c_y + c_y c_z + c_z c_x)] \tau_0 + [(c_x + c_y - 2c_z)(\eta_z^{i1} - \eta_x^{i1}) + 2\eta_z^{i2}(-2c_x c_y + c_y c_z + c_z c_x)] \tau_z / 2 + [\sqrt{3}(c_x - c_y)(\eta_z^{i1} - \eta_x^{i1} + 2c_z \eta_z^{i2})] \tau_x / 2 \}, \quad (S1)$$

with $i = E_g(d) \equiv 1, \Gamma_8(f) \equiv 2$,

$$V_{E_g-\Gamma_8}(\mathbf{k}) = -\mu_y V \{ s_x \sigma_x \tau_0 [\eta_x^{v1} + \eta_z^{v1} + 2(c_z + c_y)(\eta_z^{v2} + \eta_x^{v2})] + s_y \sigma_y \tau_0 [\eta_x^{v1} + \eta_z^{v1} + 2(c_z + c_x)(\eta_z^{v2} + \eta_x^{v2})] + s_z \sigma_z \tau_0 [\eta_x^{v1} + \eta_z^{v1} + 2(c_x + c_y)(\eta_z^{v2} + \eta_x^{v2})] + s_x \sigma_x \tau_z [-\eta_x^{v1} + \eta_z^{v1} + 2(c_z - 2c_y)(\eta_z^{v2} - \eta_x^{v2})] / 2 + s_y \sigma_y \tau_z [-\eta_x^{v1} + \eta_z^{v1} + 2(c_z - 2c_x)(\eta_z^{v2} - \eta_x^{v2})] / 2 + s_z \sigma_z \tau_z [\eta_x^{v1} - \eta_z^{v1} + (c_x + c_y)(\eta_z^{v2} - \eta_x^{v2})] + \sqrt{3} s_x \sigma_x \tau_x [\eta_x^{v1} - \eta_z^{v1} + 2c_z(\eta_z^{v2} - \eta_x^{v2})] / 2 + \sqrt{3} s_y \sigma_y \tau_x [-\eta_x^{v1} + \eta_z^{v1} - 2c_z(\eta_z^{v2} - \eta_x^{v2})] / 2 + \sqrt{3} s_z \sigma_z \tau_x (c_x - c_y)(\eta_z^{v2} - \eta_x^{v2}) \}; \quad (S2)$$

- 6-band models consisting of the $E_g(d)$ quartet interacting with the $\Gamma_7(f)$ doublet.

Here the parameters are ϵ^d , $\epsilon_7^f = \langle \Gamma_7 + |H| \Gamma_7 \rangle_{000}$, η_x^{d1} , η_z^{d1} , η_z^{d2} , $\eta_7^{f1} = \langle \Gamma_7 + |H| \Gamma_7 \rangle_{001}$, $\eta_7^{f2} = \langle \Gamma_7 + |H| \Gamma_7 \rangle_{110}$, $\eta_7^{f3} = \langle \Gamma_7 + |H| \Gamma_7 \rangle_{111}$, $\eta_7^{v1} = \langle d_{x^2-y^2} \uparrow | H | \Gamma_7 \rangle_{001}$, $\eta_7^{v2} = \langle d_{z^2} \uparrow | H | \Gamma_7 \rangle_{110}$;

and Hamiltonian $H = H_{E_g} + H_{\Gamma_7} + V_{E_g-\Gamma_7}$:

$$H_{\Gamma_7}(\mathbf{k}) = -t_{\Gamma_7}\sigma_0\mu_2[2\eta_7^{f1}(c_x + c_y + c_z) + 4\eta_7^{f2}(c_x c_y + c_y c_z + c_z c_x) + 8\eta_7^{f3}c_x c_y c_z], \quad (\text{S3})$$

$$\begin{aligned} V_{E_g-\Gamma_7}(\mathbf{k}) = & -\mu_y V\{2s_z\sigma_z\omega_0[(\eta_7^{v1} - \sqrt{3}(c_x + c_y)\eta_7^{v2}) + \\ & + (s_x\sigma_x + s_y\sigma_y)\omega_0[-\eta_7^{v1} + 2\sqrt{3}c_z\eta_7^{v2}] + \\ & + 2s_z\sigma_z\omega_1(c_y - c_x)\eta_7^{v2} + \\ & + s_x\sigma_x\omega_1[-\sqrt{3}\eta_7^{v1} + 2\eta_7^{v2}(c_z + 2c_y)] + \\ & + s_y\sigma_y\omega_1[\sqrt{3}\eta_7^{v1} - 2\eta_7^{v2}(c_z + 2c_x)]\}, \end{aligned} \quad (\text{S4})$$

where $\omega_0 = (1, 0)$ and $\omega_1 = (0, 1)$ act in the orbital space, projecting respectively onto the $d_{x^2-y^2}$ and d_{z^2} doublets, and $H_{E_g}(\mathbf{k})$ is the same as from the 8-band model;

- 4-band model consisting of conduction (s) electrons interacting with the $\Gamma_8^{(2)}(f)$ doublet.

This has parameters $\epsilon^s = \langle s|H|s\rangle_{000}$, $\epsilon^f = \langle \Gamma_8^{(2)} + |H|\Gamma_8^{(2)} + \rangle_{000}$, $\eta^{s1} = \langle s|H|s\rangle_{001}$, $\eta^{s2} = \langle s|H|s\rangle_{110}$, $\eta^{f1} = \langle \Gamma_8^{(2)} + |H|\Gamma_8^{(2)} + \rangle_{001}$, $\eta^{f2} = \langle \Gamma_8^{(2)} + |H|\Gamma_8^{(2)} + \rangle_{110}$, $\eta^{v1} = \langle s \uparrow |H|\Gamma_8^{(2)} + \rangle_{001}$: and Hamiltonian $H = H_s + H_{\Gamma_8^{(2)}} + V_{s-\Gamma_8^{(2)}}$:

$$H_i(\mathbf{k}) = -2t_i\mu_i[\eta^{i1}(c_x + c_y + c_z) + 2\eta^{i2}(c_x c_y + c_y c_z + c_z c_x)]\sigma_0, \quad (\text{S5})$$

$$V_{s-\Gamma_8^{(2)}}(\mathbf{k}) = 2V\mu_y\eta^{v1}(s_x\sigma_x + s_y\sigma_y + s_z\sigma_z), \quad (\text{S6})$$

with $i = s \equiv 1, \Gamma_8^{(2)}(f) \equiv 2$.

We now relate these general model Hamiltonians to models which have appeared in the literature and to those which are listed in Table 1 of the main text.

- The model by Legner *et al.*¹ (here abbreviated as *sf*) is identical to the 4-band model, setting $\eta^{s2}/\eta^{s1} = \eta^{f2}/\eta^{f1} \sim -0.5$.
- The 8-band model by Alexandrov *et al.*² (A^{1z}) is obtained in the E_g - Γ_8 basis by setting $\eta_z^{d1}/\eta_x^{d1} \sim \eta_z^{f1}/\eta_x^{f1} \sim -0.3$, and keeping the η_z^{v1} 1NN term in the hybridization. For completeness, we have also considered the same model with the η_x^{v2} (A^{2x}) 2NN term in the hybridization, since it belongs to a different phase.
- Our Γ_8^{1x} and Γ_8^{2z} 8-band models are obtained retaining the E_g and the Γ_8 quartets, with $\eta_z^{d2}/\eta_z^{d1} \sim -3/8$, $\eta_z^{f2}/\eta_z^{f1} \sim -1/2$ and keeping either the 1NN η_x^{v1} (Γ_8^{1x}) or the 2NN η_z^{v2} (Γ_8^{2z}) term in the hybridization.
- Our Γ_7^{1x} and Γ_7^{2z} 6-band models are obtained retaining the E_g quartet and the Γ_7 doublet, with $\eta_z^{d2}/\eta_z^{d1} \sim -3/8$, $\eta_7^{f3}/\eta_7^{f2} \sim 1/2$, and keeping either the 1NN η_7^{v1} (Γ_7^{1x}) or the 2NN η_7^{v2} (Γ_7^{2z}) term in the hybridization.

- The full tight-binding calculation (*FTB*) of Ref. 3 comprises the E_g and the Γ_8 quartets, and the Γ_7 doublet, for a total of 10 orbitals per site. Parameters are retained up to 7NN, such that we cannot give a complete analytic expression.
- The model by Takimoto⁴ (*T*) is equivalent to our $E_g - \Gamma_8$ model, retaining, however, in addition to more f terms, also the η_z^{v1} hybridization term. This term alone, in our approach, does not lead to an insulator, since it does not provide a gap along the $\Gamma - X$ direction in the BZ. Therefore we have not discussed this model in the paper.

B. Realistic tight-binding parameters

A plausible parameter set for the Γ_8^{2z} model, which essentially reproduces the DFT bandstructure of PuB_6 ,⁵ is:³ $t_d = 1 \text{ eV}$, $t_f = 0.01 \text{ eV}$, $\epsilon_8^f - \epsilon_d = -2 \text{ eV}$, $\eta_z^{d1} = 0.8$, $\eta_z^{d2} = -0.3$, $\eta_z^{f1} = -4$, $\eta_z^{f2} = 2$, $V\eta_z^{v2} = 0.06 \text{ eV}$. Similarly, a plausible parameter set for the Γ_7^{2z} model is: $t_d = 1 \text{ eV}$, $t_f = 0.01 \text{ eV}$, $\epsilon_7^f - \epsilon_d = -1.9 \text{ eV}$, $\eta_z^{d1} = 0.8$, $\eta_z^{d2} = -0.3$, $\eta_7^{f2} = 2.5$, $\eta_z^{f3} = 1.25$, $V\eta_7^{v2} = 0.05 \text{ eV}$. The effect of electronic correlations, mainly absent from DFT, will be a downward renormalization of t_f and V , see Ref. 3 for a more extensive discussion.

Panels (a) and (b) of Fig. 3 of the main text have been calculated using the sf model with $t_s = 1\text{eV}$, $t_f = 0.003\text{eV}$, $\epsilon_f - \epsilon_2 = -2\text{eV}$, $\eta^{s1} = \eta^{f1} = 1$, $\eta^{s2} = \eta^{f2} = -0.5$, $V\eta^{v1} = 0.2\text{eV}$. Panels (c) and (d) of the same figure have been obtained using the Γ_8^{2z} model with $t_d = 1\text{eV}$, $t_f = 0.01\text{eV}$, $\epsilon_8^f - \epsilon_d = -2\text{eV}$, $\eta_z^{d1} = 0.8$, $\eta_z^{d2} = -0.3$, $\eta_z^{f1} = -4$, $\eta_z^{f2} = 2$, $V\eta_z^{v2} = 0.02\text{eV}$, $V\eta_z^{v1} = -0.06\text{eV}$. Compared to the parameter set from above, this includes the additional hybridization parameter η_z^{v1} which improves the quantitative agreement with DFT, but does not change the topological properties.

II. SEV FROM MIRROR SYMMETRY EIGENVALUES

Here we show how to compute the spin expectation value (SEV) of surface states from the corresponding mirror eigenvalues. Mirror operators are defined as $M_l \equiv M_l^{orb} M_l^{spin}$, where $M_l^{orb} : l \rightarrow -l$, ($l = x, y, z$), $M_{x\pm y}^{orb} : x \leftrightarrow \mp y$, and $M_l^{spin} = e^{-i\pi\sigma_l} = -i\sigma_l$ ($l = x, y, z$), $M_{x\pm y}^{spin} = -i(\sigma_x \pm \sigma_y)/\sqrt{2} \equiv -i\sigma_{x\pm y}$.

We now determine the action of these mirror operators on E_g , Γ_7 , Γ_8 states:

$$M_l|d_m\sigma\rangle = -i\sigma_l|d_m\sigma\rangle, \quad m = x^2 - y^2, z^2; \sigma = \uparrow, \downarrow, \quad (\text{S7})$$

$$M_l|\Gamma_m\sigma\rangle = +i\sigma_l|\Gamma_m\sigma\rangle, \quad m = 8^{(1)}, 8^{(2)}, 7; \sigma = \pm, \quad (\text{S8})$$

where $l = x, y, z$, and σ_l acts on the subspace spanned by \uparrow, \downarrow for d states, or by $+, -$ for f states; moreover

$$M_{x\pm y}|d_{x^2-y^2}\sigma\rangle = +i\frac{\sigma_x \pm \sigma_y}{\sqrt{2}}|d_{x^2-y^2}\sigma\rangle, \quad (\text{S9})$$

$$M_{x\pm y}|d_{z^2}\sigma\rangle = -i\frac{\sigma_x \pm \sigma_y}{\sqrt{2}}|d_{z^2}\sigma\rangle, \quad (\text{S10})$$

$$M_{x\pm y}|\Gamma_m\sigma\rangle = -i\frac{\sigma_x \pm \sigma_y}{\sqrt{2}}|\Gamma_m\sigma\rangle, \quad m = 8^{(1)}, 7, \quad (\text{S11})$$

$$M_{x\pm y}|\Gamma_m\sigma\rangle = +i\frac{\sigma_x \pm \sigma_y}{\sqrt{2}}|\Gamma_m\sigma\rangle, \quad m = 8^{(2)}. \quad (\text{S12})$$

We can now find which states belong to eigenvalues $(\pm i)$. We start with M_x . States with eigenvalue $(-i)$ are:

$$|\psi_{1,x}^-\rangle = |d_{x^2-y^2}\rangle(1, 1)/\sqrt{2}, \quad (\text{S13})$$

$$|\psi_{2,x}^-\rangle = |d_{z^2}\rangle(1, 1)/\sqrt{2}, \quad (\text{S14})$$

$$|\psi_{3,x}^-\rangle = |\Gamma_8^{(1)}\rangle(1, -1)/\sqrt{2}, \quad (\text{S15})$$

$$|\psi_{4,x}^-\rangle = |\Gamma_8^{(2)}\rangle(1, -1)/\sqrt{2}, \quad (\text{S16})$$

$$|\psi_{5,x}^-\rangle = |\Gamma_7\rangle(1, -1)/\sqrt{2} \quad (\text{S17})$$

where the two-dimensional vector is in the (\uparrow, \downarrow) (d states) or $(+, -)$ (f states) subspace. The states $|\psi_{1,x}^- \rangle$ and $|\psi_{2,x}^- \rangle$ are spin eigenstates, pointing towards the positive x ($+x$) direction, but the other three states are not, because $+$ and $-$ are not spin indices. We can, however, compute the SEV on these states with

the use of Table S1. Now, on Γ_8 states, $\langle\sigma_x, \sigma_y, \sigma_z\rangle \sim (-\hat{s}_x, -\hat{s}_y, -\hat{s}_z)$, where on the left-hand side σ_i are true spin operators, while on the right-hand side \hat{s}_i act on the pseudospin space; for Γ_7 states, instead, $\langle\sigma_x, \sigma_y, \sigma_z\rangle \sim (+\hat{s}_x, +\hat{s}_y, +\hat{s}_z)$. So, for states $|\psi_{3,x}^- \rangle$ and $|\psi_{4,x}^- \rangle$ the SEV is pointing in the $+x$ direction, while for $|\psi_{5,x}^- \rangle$ it is pointing in the $-x$ direction.

To conclude, for a state $|\psi\rangle$ with $M_x|\psi\rangle = -i|\psi\rangle$, even though it is not in general an eigenstate of the spin, its SEV is pointing along $+x$ if it is a d or a Γ_8 state, but along $-x$ if it is a Γ_7 state. The opposite holds for eigenvalue $+i$. We can repeat the same reasoning for M_y , and conclude that, for a state $|\psi\rangle$ with $M_y|\psi\rangle = -i|\psi\rangle$ its SEV is pointing along $+y$ if it is a d or a Γ_8 state, but along $-y$ if it is a Γ_7 state.

For M_{x-y} the eigenstates with eigenvalue $(-i)$ are:

$$|\psi_{1,x-y}^-\rangle = |d_{x^2-y^2}\rangle(1, \epsilon^{3i\pi/4})/\sqrt{2}, \quad (\text{S18})$$

$$|\psi_{2,x-y}^-\rangle = |d_{z^2}\rangle(1, \epsilon^{-i\pi/4})/\sqrt{2}, \quad (\text{S19})$$

$$|\psi_{3,x-y}^-\rangle = |\Gamma_8^{(1)}\rangle(1, \epsilon^{-i\pi/4})/\sqrt{2}, \quad (\text{S20})$$

$$|\psi_{4,x-y}^-\rangle = |\Gamma_8^{(2)}\rangle(1, \epsilon^{3i\pi/4})/\sqrt{2}, \quad (\text{S21})$$

$$|\psi_{5,x-y}^-\rangle = |\Gamma_7\rangle(1, \epsilon^{-i\pi/4})/\sqrt{2}, \quad (\text{S22})$$

which means that $|\psi_{1,x-y}^- \rangle$ is a spin eigenstate with spin pointing along $(-x + y)$, while $|\psi_{2,x-y}^- \rangle$ points along $(x - y)$; for $|\psi_{3,x-y}^- \rangle$ the SEV points along $(-x + y)$, for $|\psi_{4,x-y}^- \rangle$ along $(x - y)$, and for $|\psi_{5,x-y}^- \rangle$ along $(x - y)$.

From this we read off that for a state $|\psi\rangle$ with $M_{x-y}|\psi\rangle = -i|\psi\rangle$ the SEV points along $(x - y)$ if it is d_{z^2} , $\Gamma_8^{(2)}$ or Γ_7 , and along $(-x + y)$ if it is $d_{x^2-y^2}$ or $\Gamma_8^{(1)}$. Similarly, for a state $|\psi\rangle$ with $M_{x+y}|\psi\rangle = -i|\psi\rangle$ the SEV points along $(x + y)$ if it is d_{z^2} , $\Gamma_8^{(2)}$ or Γ_7 , and along $(-x - y)$ if it is $d_{x^2-y^2}$ or $\Gamma_8^{(1)}$. This concludes the set of rules used in the main text.

In addition, the 4-band model requires s and $\Gamma_8^{(2)}$ states: s states behave as d_{z^2} states, so if $M_x|\psi\rangle = -i|\psi\rangle$, the spin points along $+x$, if $M_y|\psi\rangle = -i|\psi\rangle$, it points along $+y$, and if $M_{x-y}|\psi\rangle = -i|\psi\rangle$, the spin points along $(+x - y)$. As for $\Gamma_8^{(2)}$, if $M_x|\psi\rangle = -i|\psi\rangle$, the SEV points along $+x$, if $M_y|\psi\rangle = -i|\psi\rangle$, it points along $+y$, and if $M_{x-y}|\psi\rangle = -i|\psi\rangle$, it points along $(+x - y)$. We note that the transformation $x \rightarrow -x$, $y \rightarrow -y$, needed to obtain the hybridization term Eq. (S6) with all plus signs, changes the explicit form of $\Gamma_8^{(2)}$ states, but neither their symmetries properties nor their SEV.

III. SYMMETRY OF SURFACE STATES AT $\bar{\Gamma}$

In this section we show how v determines the symmetry of the states which build the $\bar{\Gamma}$ cone for small momenta.

As usual⁶ we introduce a time-reversal doublet $|\psi_+\rangle$, $|\psi_-\rangle$ which describes surface states at $\bar{\Gamma}$; it can be writ-

$(\sigma^x, \sigma^y, \sigma^z)$	$\Gamma_8^{(1)+}$	$\Gamma_8^{(1)-}$	$\Gamma_8^{(2)+}$	$\Gamma_8^{(2)-}$	Γ_7+	Γ_7-
$\Gamma_8^{(1)+}$	$\frac{11}{21}(0, 0, -1)$	$\frac{5}{21}(-1, i, 0)$	$(0, 0, 0)$	$\frac{2\sqrt{3}}{21}(-1, -i, 0)$	$\frac{4\sqrt{5}}{21}(0, 0, -1)$	$\frac{2\sqrt{5}}{21}(1, -i, 0)$
$\Gamma_8^{(1)-}$	$\frac{5}{21}(-1, -i, 0)$	$\frac{11}{21}(0, 0, 1)$	$\frac{2\sqrt{3}}{21}(-1, i, 0)$	$(0, 0, 0)$	$\frac{2\sqrt{5}}{21}(1, i, 0)$	$\frac{4\sqrt{5}}{21}(0, 0, 1)$
$\Gamma_8^{(2)+}$	$(0, 0, 0)$	$\frac{2\sqrt{3}}{21}(-1, -i, 0)$	$\frac{1}{7}(0, 0, -1)$	$\frac{3}{7}(-1, i, 0)$	$(0, 0, 0)$	$\frac{2\sqrt{15}}{21}(1, i, 0)$
$\Gamma_8^{(2)-}$	$\frac{2\sqrt{3}}{21}(-1, i, 0)$	$(0, 0, 0)$	$\frac{3}{7}(-1, -i, 0)$	$\frac{1}{7}(0, 0, 1)$	$\frac{2\sqrt{15}}{21}(1, -i, 0)$	$(0, 0, 0)$
Γ_7+	$\frac{4\sqrt{5}}{21}(0, 0, -1)$	$\frac{2\sqrt{5}}{21}(1, -i, 0)$	$(0, 0, 0)$	$\frac{2\sqrt{15}}{21}(1, i, 0)$	$\frac{5}{21}(0, 0, 1)$	$\frac{5}{21}(1, -i, 0)$
Γ_7-	$\frac{2\sqrt{5}}{21}(1, i, 0)$	$\frac{4\sqrt{5}}{21}(0, 0, 1)$	$\frac{2\sqrt{15}}{21}(1, -i, 0)$	$(0, 0, 0)$	$\frac{5}{21}(1, i, 0)$	$\frac{5}{21}(0, 0, -1)$

Table S1. SEV in the $\Gamma_7 - \Gamma_8$ basis.

ten as:

$$|\psi_+\rangle = \phi_1|d_{x^2-y^2} \uparrow\rangle + \phi_2|d_{z^2} \uparrow\rangle + \phi_3|\Gamma_8^{(1)+}\rangle + \phi_4|\Gamma_8^{(2)+}\rangle + \phi_5|\Gamma_7+\rangle, \quad (\text{S23})$$

$$|\psi_-\rangle = \phi_1|d_{x^2-y^2} \downarrow\rangle + \phi_2|d_{z^2} \downarrow\rangle - \phi_3|\Gamma_8^{(1)-}\rangle - \phi_4|\Gamma_8^{(2)-}\rangle - \phi_5|\Gamma_7-\rangle. \quad (\text{S24})$$

$$(\text{S25})$$

It is constructed such that

$$\langle(\sigma_x, \sigma_y, \sigma_z)\rangle = (a\hat{s}_x, a\hat{s}_y, b\hat{s}_z), \quad (\text{S26})$$

with a and b real numbers, as can be seen through the use of Table S1, and where we suppose that the Γ_8 coefficients ϕ_3, ϕ_4 and the Γ_7 one ϕ_5 are not non-zero at the same time. The eigenstate with positive energy for the Dirac Hamiltonian $H_{\bar{\Gamma}} = v_0 w(k_x \sigma_y - k_y \sigma_x)$ with $w = +1$ is now

$$|\phi^+(\theta_{\mathbf{k}})\rangle = \frac{1}{\sqrt{2}}(|\psi_+\rangle + i\epsilon^{i\theta_{\mathbf{k}}}|\psi_-\rangle), \quad (\text{S27})$$

$$\cos \theta_{\mathbf{k}} = \frac{k_x}{k}, \quad \sin \theta_{\mathbf{k}} = \frac{k_y}{k}. \quad (\text{S28})$$

This state has the properties

$$M_y|\phi^+(0)\rangle = -i|\phi^+(0)\rangle, \quad (\text{S29})$$

$$M_x|\phi^+(\pi/2)\rangle = +i|\phi^+(\pi/2)\rangle, \quad (\text{S30})$$

$$M_{x-y}|\phi^+(\pi/4)\rangle = -i|\phi^+(\pi/4)\rangle, \quad \phi_2, \phi_4 = 0, \quad (\text{S31})$$

$$M_{x-y}|\phi^+(\pi/4)\rangle = +i|\phi^+(\pi/4)\rangle, \quad \phi_1, \phi_3, \phi_5 = 0. (\text{S32})$$

We now see that when $w = +1, v = +1$, we must have $M_{x-y}|\phi^+(\pi/4)\rangle = +i|\phi^+(\pi/4)\rangle$, so, in this case, the $\bar{\Gamma}$ cone is entirely composed by d_{z^2} and $\Gamma_8^{(2)}$; however, when $w = +1, v = -1$, we must have $M_{x-y}|\phi^+(\pi/4)\rangle = -i|\phi^+(\pi/4)\rangle$, so the $\bar{\Gamma}$ cone is now entirely composed by $d_{x^2-y^2}, \Gamma_8^{(1)}$ and Γ_7 . For $w = -1$ all mirror eigenvalue signs and spin directions are reversed, but the results are the same. We conclude that v dictates the symmetry of the surface states at $\bar{\Gamma}$ for small momenta.

¹ M. Legner, A. Rüegg, and M. Sigrist, Phys. Rev. B **89**, 085110 (2014).

² V. Alexandrov, M. Dzero, and P. Coleman, Phys. Rev. Lett. **111**, 226403 (2013).

³ P. P. Baruselli and M. Vojta, Phys. Rev. B **90**, 201106 (2014).

⁴ T. Takimoto, J. Phys. Soc. Jpn. **80**, 123710 (2011).

⁵ X. Deng, K. Haule, and G. Kotliar, Phys. Rev. Lett. **111**, 176404 (2013).

⁶ C.-X. Liu, X.-L. Qi, H. Zhang, X. Dai, Z. Fang, and S.-C. Zhang, Phys. Rev. B **82**, 045122 (2010).